# Slow Inhibition and Conformation Selective Properties of Extracellular Signal-Regulated Kinase 1 and 2 Inhibitors

Johannes Rudolph,[†,‡] Yao Xiao,[†,‡] Arthur Pardi,[†] and Natalie G. Ahn*,[†,‡,§]

[†]Department of Chemistry and Biochemistry, [‡]Howard Hughes Medical Institute, and [§]BioFrontiers Institute, University of Colorado, Boulder, Colorado 80309, United States

**S** *Supporting Information*

**ABSTRACT:** The mitogen-activated protein (MAP) kinase pathway is a target for anticancer therapy, validated using inhibitors of B-Raf and MAP kinase kinase (MKK) 1 and 2. Clinical outcomes show a high frequency of acquired resistance in patient tumors, involving upregulation of activity of the MAP kinase, extracellular signal-regulated kinase (ERK) 1 and 2. Thus, inhibitors for ERK1/2 are potentially important for targeted therapeutics against cancer. The structures and potencies of different ERK inhibitors have been



published, but their kinetic mechanisms have not been characterized. Here we perform enzyme kinetic studies on six representative ERK inhibitors, with potencies varying from 100 pM to 20 $\mu$M. Compounds with significant biological activity (IC$_{50}$ < 100 nM) that inhibit in the subnanomolar range (Vertex-11e and SCH772984) display slow-onset inhibition and represent the first inhibitors of ERK2 known to demonstrate slow dissociation rate constants (values of 0.2 and 1.1 h$^{-1}$, respectively). Furthermore, we demonstrate using kinetic competition assays that Vertex-11e binds with differing affinities to ERK2 in its inactive, unphosphorylated and active, phosphorylated forms. Finally, two-dimensional heteronuclear multiple-quantum correlation nuclear magnetic resonance experiments reveal that distinct conformational states are formed in complexes of Vertex-11e with inactive and active ERK2. Importantly, two conformers interconvert in equilibrium in the active ERK2 apoenzyme, but Vertex-11e strongly shifts the equilibrium completely to one conformer. Thus, a high-affinity, slow dissociation inhibitor stabilizes different enzyme conformations depending on the activity state of ERK2 and reveals properties of conformational selection toward the active kinase.
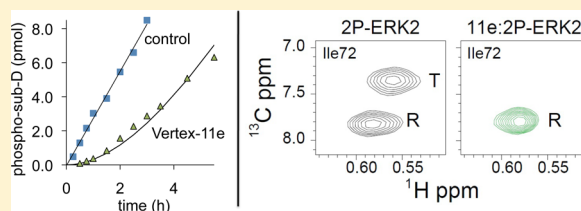
The mitogen-activated protein (MAP) kinase pathway is a compelling target for anticancer therapy given the prevalence of oncogenic RAS and B-RAF in many cancer types.[1] Small molecule inhibitors specifically targeting B-RAF and MAP kinase kinase 1 and 2 (MKK1/2) in the MAP kinase pathway have been recently approved for the treatment of patients with metastatic melanomas harboring B-RAF$^{V600E}$ activating mutations.[2] However, while clinical outcomes show impressive disease free survival for a median of 6−7 months with single-line treatment and 13 months using combination therapy with inhibitors of BRAF (dabrafenib) and MKK1/2 (trametinib), nearly all patients eventually relapse.[3−5] Because of the prevalence of acquired resistance and the ensuing high patient mortality, alternative strategies for targeted therapeutics are an imperative goal.

Many tumors with acquired resistance show an increased copy number or alternative splicing of B-RAF$^{V600E}$, activating mutations in K-RAS, N-RAS, or MKK1/2, or elevated levels of expression of MAP kinases or receptor tyrosine kinases.[6−9] In these cases, resistance can be attributed to reactivation of the MAP kinase, extracellular signal-regulated kinase 1 and 2 (ERK1/2).[8,9] For this reason, ERK is an increasingly attractive target for therapeutics. In recent publications, ERK inhibitors (SCH772984 and ERK-i) have shown efficacy in blocking growth of cancer cell lines with acquired resistance to B-RAF and MKK inhibitors.[10,11] Both SCH772984 and Vertex-11e, a

compound closely related to ERK-i, have been reported to be potent inhibitors *in vitro* ($K_d$ values of 0.19 and 0.11 nM, respectively) and *in vivo* (IC$_{50}$ values of 60 and 48 nM, respectively).[10,12] However, to date, the kinetic properties of these molecules toward active ERK2 have not been compared to those of other inhibitors of ERK, and thus, the basis for their potency remains unknown.

ERK1 and -2 are activated by dual phosphorylation at Thr and Tyr residues within the activation loop, both events catalyzed by MKK1/2. X-ray structures of unphosphorylated ERK2 ("0P-ERK2") and dually phosphorylated ERK2 ("2P-ERK2") show that phosphorylation rearranges the activation loop to organize residues in the active site and allow productive recognition of substrates containing the phosphorylation motif, Pro-Xxx-pSer/pThr-Pro.[13,14] However, overall structural changes within the active site of ERK2 are relatively modest, and it is unclear what additional features may explain the >500000-fold increase in $k_{cat}/K_m$ induced by phosphorylation.[15] Using nuclear magnetic resonance (NMR) relaxation dispersion experiments, we have recently discovered that dual

phosphorylation of ERK2 induces significant changes in the dynamics of the enzyme.[16] Whereas 0P-ERK2 exists as one major conformer, 2P-ERK2 exists in two separate conformers that exchange on a millisecond time scale. The minor (20%) conformer in 2P-ERK2 corresponds to the conformer seen in 0P-ERK2, while the major (80%) conformer in 2P-ERK2 represents a new form that is energetically inaccessible in 0P-ERK2. Thus, a major effect of ERK2 phosphorylation is to alter the dynamics of the enzyme, lowering the thermodynamic barrier to allow formation of a new conformer, which is accessible only in the activated state.

Such allosteric behavior of ERK2 suggests its possible exploitation by inhibitors with conformation selective properties. Conformational selection is emerging as an important property of certain kinase inhibitors, termed "type II", which work by trapping nonproductive active site conformers. This was first shown for BCR-ABL kinase inhibitors (e.g., imatinib and posatinib), which induce a "DFG flip" where Asp and Phe side chains in the conserved DFG motif swap positions to form an inactive "DFG-out" conformer.[17,18] In contrast to "DFG-out", the EGF receptor inhibitor lapatinib binds an inactive "helix $\alpha$C-out" conformer, disrupting the $Mg^{2+}$-coordinating Lys-Glu ion pair.[19,20] In each case, the allosteric effects of type II inhibitors reinforce their ATP competitive effects.

Here we characterize the kinetics of inhibition by small molecules that target ERK1/2. Importantly, we show that two inhibitors (Vertex-11e and SCH772984), which have the greatest reported cellular efficacy, show slow binding and slow dissociation from ERK2. Slow dissociation is an important property that predicts higher drug potency because of greater cellular retention.[21,22] Using NMR, we show that Vertex-11e is able to trap ERK2 into different conformations depending on the kinase activity state. Importantly, the thermodynamic equilibrium between conformers seen in 2P-ERK2 is shifted completely to one form upon Vertex-11e binding. Our results indicate that phosphorylation-induced dynamics introduces an allosteric property into ERK2 that can be exploited for conformation selective inhibition.

## ■ MATERIALS AND METHODS

**Materials.** Rat ERK2 was expressed in *Escherichia coli* in its inactive, unphosphorylated form (0P-ERK2) and phosphorylated with the active mutant MKK1-G7B to produce the active, stoichiometrically dually phosphorylated form (2P-ERK2) as previously described.[23,24] Vertex-11e was purchased from Chemie-Tek. SCH772984 was purchased from Cedarlane Laboratories. Vertex-1 and FR180204 were purchased from Key Organics. ATP, SB220025, and olomoucin were purchased from Sigma-Aldrich.

**Enzyme Kinetics.** Kinase activity was measured by $^{32}P$ phosphoryl transfer from $[\gamma\text{-}^{32}P]ATP$ (1.7−5 Ci/mmol, PerkinElmer) to the peptide substrate, sub-D (Anaspec). Reactions were conducted at 25 °C in 25 mM HEPES (pH 7.4), 10 mM $MgCl_2$, 100 mM NaCl, 1 mM dithiothreitol, and 0.02% Tween 20. ATP concentrations were varied from 3 to 500 $\mu$M for measurements of inhibitor $K_i$ and held fixed at 100 and 500 $\mu$M for measurements of inhibitor association and dissociation kinetics, respectively. Concentrations of sub-D were varied from 0.06 to 20 $\mu$M for measurements of $K_m$ and held fixed at 20 $\mu$M for all assays using inhibitors. Inhibitor concentrations were varied as follows: olomoucin, 1−250 $\mu$M; SB220025, 2−150 $\mu$M; FR180204, 16−8000 nM; Vertex-1, 0.04−40 $\mu$M; Vertex-11e, 0.5−200 nM, and SCH772984, 0.5−
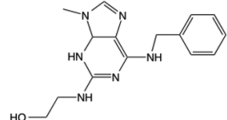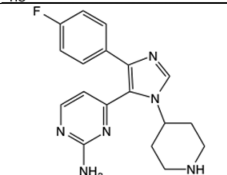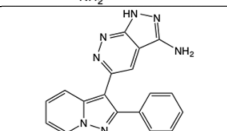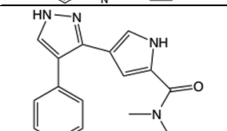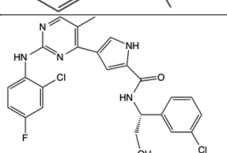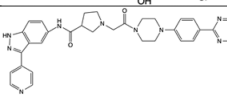
100 nM. Reactions with volumes of 10−20 $\mu$L were run in 96-well V-bottom polystyrene plates (Costar 3897) and quenched with a 10−20-fold excess volume of 200 mM phosphoric acid. The phosphorylated peptide was separated from ATP in a 96-well filter binding apparatus (S&S Minifold I) using P81 ion exchange paper (Whatman). The filter paper was washed in the apparatus with 3 × 150 $\mu$L of 200 mM phosphoric acid and then washed in a tray with 3 × 20 mL of phosphoric acid. The phosphorylated peptide was detected by exposure of the filter paper to a phosphoimager plate (GE Healthcare) and quantified using ImageQuant (GE Healthcare). Data fitting was performed by least-squares minimization using Microsoft Excel.

For all $K_D$ experiments involving tight-binding inhibitors, activity determinations were performed as described above, adding 10× concentrated solutions of ATP and sub-D to initiate the reaction, and using a short reaction time (15 s). In this way, the activity measurements best reflect the equilibrium established during the preincubation. For experiments determining the $K_i$ values of Vertex-11e and SCH772984, the inhibitor concentrations were varied from 3 to 200 nM, preincubating each inhibitor for 30 min with 10−100 nM 2P-ERK2. For the measurements of tight-binding inhibitor interactions with 0P-ERK2, the concentrations of Vertex-11e and SCH772984 were held fixed at 1 and 8 nM, respectively, preincubating each for 30 min with mixtures of 0P-ERK2 (0.2−200 nM) and 2P-ERK2 (4 nM).

**NMR Spectroscopy.** [*methyl*-$^1H$,$^{13}C$]Ile-, Leu-, and Val-labeled 0P- and 2P-ERK2 were prepared as previously described[16] in a buffer containing 50 mM Tris (pH 7.4), 150 mM NaCl, 5 mM $MgSO_4$, 0.1 mM EDTA, 5 mM dithiothreitol, 100% $D_2O$, and 2.5% (v/v) glycerol. Vertex-11e was prepared in a 2.5 mM stock solution in $d_6$-DMSO, because of its limited solubility in $D_2O$. Vertex-11e ($d_6$-DMSO) was then added to isotopically labeled 2P-ERK2 (40 $\mu$M) or 0P-ERK2 (30 $\mu$M), to form complexes with a 50% binding stoichiometry ([11e]: [protein] = 0.5:1) and a 100% binding stoichiometry ([11e]: [protein] = 1.2:1). The $d_6$-DMSO concentration in the final protein sample was ∼1%.

Two-dimensional (2D) $^{13}C$−$^1H$ HMQC spectra of 0P-ERK2 and 2P-ERK2 were collected on Varian VNMRS 800 and 900 MHz NMR spectrometers, respectively. Data were collected at 25 °C (8 h for 0P-ERK2 and 11 h for 2P-ERK2) and at 5 °C (12 h for 0P-ERK2 and 18 h for 2P-ERK2). Each spectrum was acquired with 144 (800 MHz) or 160 complex points (900 MHz) in the $t_1$ ($^{13}C$) dimension, corresponding to 28.8 ms at 800 MHz and 29.1 ms at 900 MHz, and 1024 complex points in the acquisition period. WURST40 $^{13}C$ decoupling was applied during the 85 ms acquisition period, and a 1.5 s delay period was used between each scan. The spectra were processed using the software package NMRPipe.[25] Time domain data in the $^1H$ dimension were apodized by a cosine-squared window function and zero-filled prior to Fourier transformation. The indirect dimension ($^{13}C$) was apodized by a cosine window function and zero-filled prior to Fourier transformation. Spectral visualization and analysis were achieved using CCPNMR Analysis software.[26] Chemical shift perturbations upon Vertex-11e binding were calculated by overlaying the 2D $^{13}C$−$^1H$ NMR spectra of 11e-bound and free forms of ERK2. In crowded regions of the spectra, the methyl peaks corresponding to the ligand-bound enzyme were assigned as the new peaks that appeared closest to the methyl peaks corresponding to the free enzyme. In this way, the chemical

**Table 1. Kinetic Parameters for Inhibition of 2P-ERK2**

| Inhibitor | Structure | IC$_{50}$ (nM) Published previously | IC$_{50}$ (nM)[a] This study | $k_{on}$ ($\mu$M$^{-1}$s$^{-1}$)[b] | $k_{off}$ (h$^{-1}$)[b] | $k_{off}/k_{on}$ (nM) | K$_i$ (nM)[c] |
|---|---|---|---|---|---|---|---|
| Olomoucin |  | 27,000 (ref 27) | 33,000 ± 3,500 | n.d. | n.d. | n.d. | 10,800 ± 2700 |
| SB220025 |  | 18,000 (ref 27) | 7,200 ± 1,400 | n.d. | n.d. | n.d. | 19,000 ± 1,000 |
| FR180204 |  | 140 (ref 28) | 330 ± 64 | > 0.8[d] | n.d. | n.d. | 63 ± 17 |
| Vertex-1 |  | 2,300 (ref 29) | 2,500 ± 550 | n.d. | n.d. | n.d. | 380 ± 86 |
| Vertex-11e |  | <2 (ref 12) | n.d. | 0.21 ± 0.04 | 0.21 ± 0.07 | 0.28 ± 0.073 | 0.34 ± 0.099 (2P); 2.5 ± 0.5 (0P) |
| SCH772984 |  | 0.24 (ref 10) | n.d. | 2.8 ± 0.34 | 1.1 ± 0.31 | 0.11 ± 0.021 | 0.12 ± 0.10 (2P); 0.12 ± 0.04 (0P) |

[a]Errors were derived from fits of duplicate experiments using eq 1. [b]Errors were derived from fits of three or more experiments. [c]All measurements describe 2P-ERK2, except where noted for Vertex-11e and SCH772984. Errors for olomoucin, SB220025, FR180204, and Vertex-1 were derived from fits of of duplicate experiments. Errors for Vertex-11e and SCH772984 were derived from fits of three or more experiments. [d]FR180204 has a dissociation rate constant of >0.05 s$^{-1}$ ($t_{1/2} < 14$ s); therefore, its rate constant for association must be >0.8 $\mu$M$^{-1}$ s$^{-1}$.

shift perturbation values represent minimum estimates. The combined $^{13}$C and $^1$H chemical shift perturbation (in parts per million) upon binding of Vertex-11e to 0P- or 2P-ERK2 was calculated by the equation $\Delta\delta_{C,H} = (\Delta\delta_{H}^2 + 0.25\Delta\delta_{C}^2)^{1/2}$, where $\Delta\delta$H and $\Delta\delta$C are the chemical shift perturbations on the proton and carbon dimensions, respectively.

## ■ RESULTS

We performed enzyme assays to examine the kinetic characteristics of six small molecule inhibitors of ERK2 (Table 1). The structures of all of these compounds have been determined crystallographically in complex with 0P-ERK2 and shown to occupy the ATP binding site between N- and C-terminal lobes (Figure 1A−G).[27−30] A medium throughput assay for 2P-ERK2 activity was developed in 96-well plates using [$\gamma$-$^{32}$P]ATP and the peptide substrate sub-D. Sub-D has a docking site derived from yeast STE7, which is linked to a C-terminal MAPK phosphorylation consensus sequence by a flexible hydrophobic linker.[32,33] It has been previously shown to be an excellent substrate for 2P-ERK2, with $k_{cat}$ values of 3−15 s$^{-1}$ and a $k_{cat}/K_m$ of ∼5 $\mu$M$^{-1}$ s$^{-1}$, comparable to those of the Ets-1 protein substrate.[32] Using 2P-ERK2, we measured a $k_{cat}$ of 4.3 ± 1.7 s$^{-1}$ and a $k_{cat}/K_{m,sub-D}$ of 4.5 ± 0.9 $\mu$M$^{-1}$ s$^{-1}$, in good agreement with literature values (Figure S1A of the Supporting Information). We also measured a $K_{m,ATP}$ of 78 ± 30 $\mu$M, in

agreement with previous reports (64 $\mu$M[15]) (Figure S1B of the Supporting Information). Using ATP and sub-D, assays were performed within the linear range of product formation over time courses of 0−8 h with 5 pM kinase and 0−60 s with 5 nM kinase.

We examined the time dependence of inhibition by olomoucin, SB220225, FR180204, and Vertex-1, initiating the reactions by addition of enzyme to a mixture of ATP, sub-D, and each inhibitor. Each experiment showed linear accumulation of the product over 10 min at varying inhibitor concentrations, as expected for rapidly binding inhibitors (Figure 2A and Figures S2A−S4A of the Supporting Information). IC$_{50}$ values were derived using eq 1:

$$\frac{v_i}{v_0} = \frac{1}{1 + \frac{[I]}{IC_{50}}}$$

(1)

where $v_i$ and $v_0$ are the observed rates measured in the presence and absence of each inhibitor, respectively, and [I] is the inhibitor concentration. The resulting IC$_{50}$ measurements for these compounds were in agreement with literature values (Table 1).

We next examined reversibility of inhibition for olomoucin, SB220225, FR180204, and Vertex-1 by preincubating the enzyme with each inhibitor followed by 300-fold dilution into
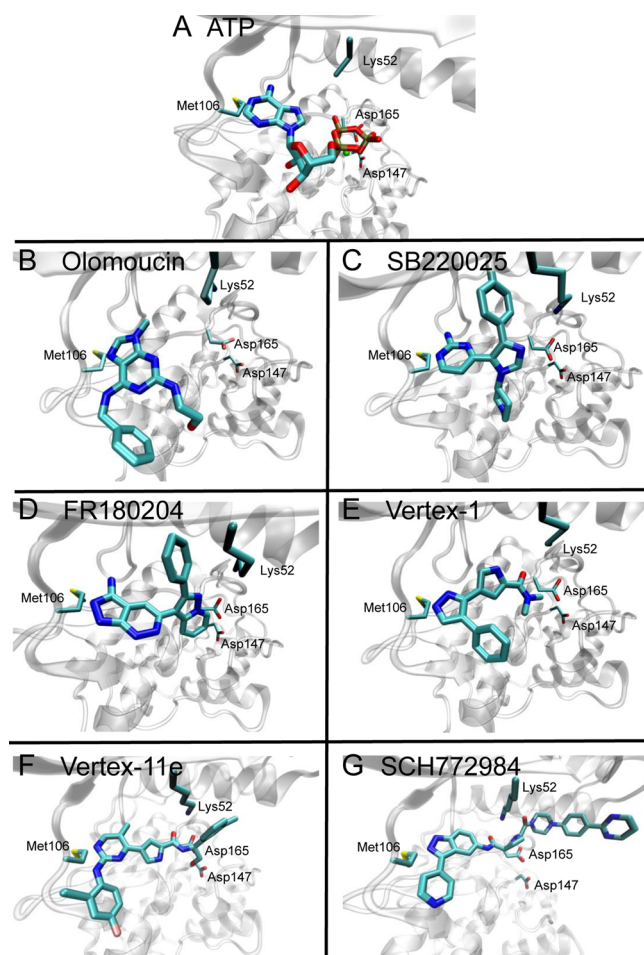
**Figure 1.** Active site of ERK2 in complex with ATP and inhibitors. Shown are X-ray structures of 0P-ERK2 bound to (A) ATP (PDB entry 4GT3), (B) olomoucin (PDB entry 4ERK), (C) SB220025 (PDB entry 3ERK), (D) FR180204 (PDB entry 1TVO), (E) Vertex-1 (PDB entry 1OJG), (F) Vertex-11e (PDB entry 4QTE), and (G) SCH772984 (PDB entry 4QTA). Key residues involved in ATP binding (Lys52, Met106, and Asp165) and the catalytic base (Asp147) are shown. In the ATP cocrystal structure, the Lys52 side chain is partially disordered. Graphics were prepared in VMD.[31]



**Figure 2.** Representative data for time-dependent assays of rapid on/off inhibitors of ERK2, FR180204. (A) Reactions were initiated by addition of 2P-ERK2 (0.25 nM) in the presence of 20 μM sub-D, 100 μM ATP, and varying concentrations of FR180204. Data were fit with a linear function. (B) Reactions were initiated by 300-fold dilution of a mixture containing 25 nM ERK2 and 4 μM FR180204 into solutions containing 20 μM sub-D and 500 μM ATP. Data were fit with a linear function. (C) Lineweaver–Burk plot for the rapidly reversible inhibitor, FR180204. 2P-ERK2 (1.25 nM) was assayed in the presence of 20 μM sub-D at varying concentrations of ATP (15–500 μM) and FR180204 (32–2000 nM) in a fixed time point assay (5 min). The inset shows the dependence of the apparent $K_m$ on the inhibitor concentration. Data were simultaneously fit using eight different instances of the Michaelis–Menten equation.

assay buffer containing ATP and sub-D substrate. Rapid recovery of activity was observed upon dilution with each inhibitor, as evidenced by linear accumulation of product over time, with rates identical to those from the control experiment without inhibitor (Figure 2B and Figures S2B–S4B of the Supporting Information). This indicates that compounds that bind rapidly to the enzyme also show rapid release. With the knowledge that olomoucin, SB220225, FR180204, and Vertex-1 are rapid on/off inhibitors, we could measure the affinity ($K_i$ = $K_d$) of these compounds for 2P-ERK2, using a fixed time point assay at varying inhibitor concentrations and varying ATP. Lineweaver–Burk replots showed that each inhibitor was competitive versus ATP (Figure 2C and Figures S2C–S4C of the Supporting Information), consistent with their occupancy of the ATP site in each crystal structure (Figure 1B–E). Replots of calculated $K_m$ values as a function of inhibitor concentration (Figure 2C, inset, and Figures S2C–S4C of the Supporting Information, inset) yielded $K_i$ values varying from 63 nM to 19 μM (Table 1).

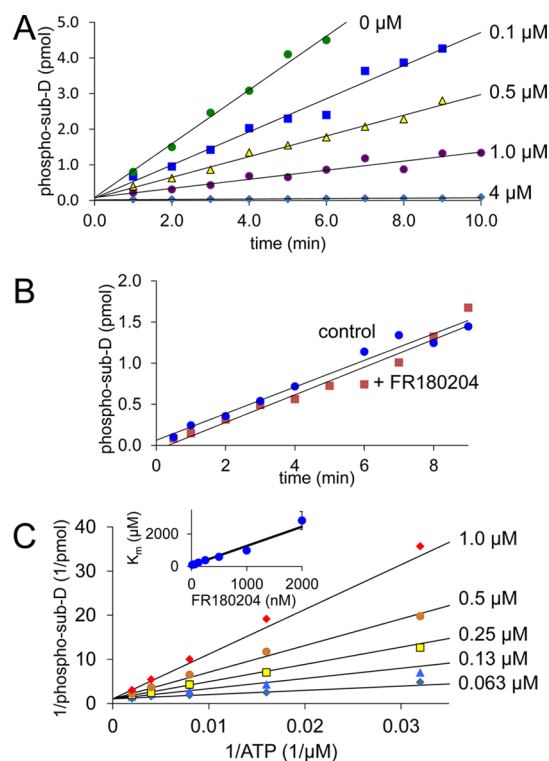Unexpectedly, when enzyme was added to Vertex-11e or SCH772984, the time dependence of product accumulation

showed strong curvature, revealing a striking hysteretic effect with each inhibitor (Figure 3A and Figure S5 of the Supporting Information). This behavior is diagnostic of slow-onset inhibition, wherein the equilibrium between free and enzyme-bound inhibitor is established slowly compared to the time scale of enzymatic turnover.[34] Product accumulation (P) during slow-onset inhibition can be fit by eq 2:[35]

$$P = \frac{v_0}{k_{obs}}(1 - e^{-k_{obs}t}) + C \tag{2}$$

where $v_0$ is the initial velocity observed upon initiation of the reaction with enzyme, $k_{obs}$ is the rate constant for the approach to complete inhibition, and $C$ is a constant to account for the background signal. Replots of $k_{obs}$ (from eq 2) versus inhibitor concentration (Figure 3A, inset, and Figure S5 of the Supporting Information, inset) were linear, supporting a one-step binding model. The slope of this line yielded estimates of $k_{on}$, the apparent rate constant for association of inhibitor with enzyme (Table 1). Vertex-11e and SCH772984 showed apparent $k_{on}$ values of 0.21 and 2.8 μM$^{-1}$ s$^{-1}$, respectively, both of which were slower than the rate of free diffusion. Thus, Vertex-11e and SCH772984 could be distinguished from the other compounds by their slow-onset inhibition. Such
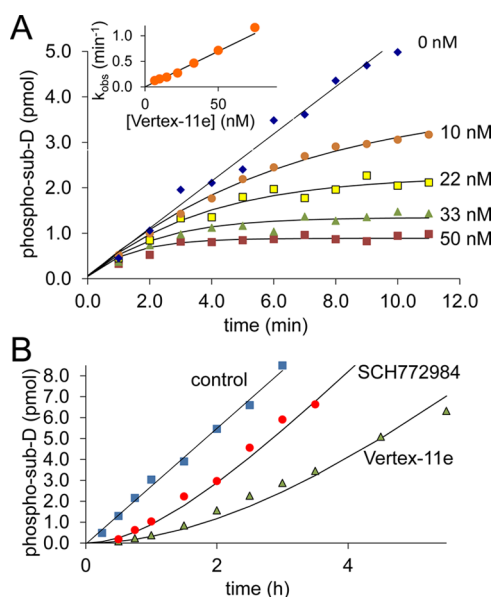
**Figure 3.** Representative time-dependent data for a slow inhibitor of ERK2, Vertex-11e. (A) Reactions were initiated by adding 2P-ERK2 (0.25 nM) with 20 $\mu$M sub-D and 100 $\mu$M ATP at varying concentrations of Vertex-11e. Data were fit using eq 2. (B) Reactions were initiated by diluting a mixture containing 2.5 nM ERK2 and 16 nM Vertex-11e by 300-fold into solutions containing 20 $\mu$M sub-D and 500 $\mu$M ATP. Data were fit using eq 2.



**Figure 4.** Representative data for the Morrison experiment with Vertex-11e or SCH772984. (A) 2P-ERK2 was preincubated with inhibitor, using 90 and 11 nM enzyme for Vertex-11e and SCH772984, respectively. Assays were initiated by adding a 10% volume of sub-D and ATP to final concentrations of 20 $\mu$M sub-D and 100 $\mu$M ATP. Data were fit using eq 3. (B) Representative data for a "double-Morrison experiment" developed to determine the affinity of Vertex-11e and SCH772984 for 0P-ERK2. Mixtures of 2P-ERK2 (4 nM) with varying concentrations of 0P-ERK2 were each preincubated with 8 nM inhibitor. Assays were initiated by adding a 10% volume of sub-D and ATP to final concentrations of 20 $\mu$M sub-D and 100 $\mu$M ATP. Data were fit using two instances of eq 3, which were simultaneously minimized to determine $K_d$ values for 0P- and 2P-ERK2. In both panels A and B, the x-axis is plotted on a log scale.

hysteresis is common for tight-binding inhibitors, although its physical origins are poorly understood.[36]

Preincubation/dilution experiments were then performed to measure the release of Vertex-11e and SCH772984 from the enzyme ($k_{off}$). Both inhibitors showed slow recovery of product formation on a time scale of hours (Figure 3B). Product accumulation curves were fit by eq 2, where $v_r$, the final observed velocity, is used in place of $v_0$. Under the conditions of the experiment, $k_{off}$ is essentially equal to $k_{obs}$, yielding dissociation rate constants for Vertex-11e and SCH772984 of 0.21 and 1.1 h$^{-1}$, respectively (Table 1). In this manner, the experimentally determined values of $k_{on}$ and $k_{off}$ could be used to calculate binding affinity constants ($K_d = k_{off}/k_{on}$) of 0.28 and 0.11 nM for Vertex-11e and SCH772984, respectively (Table 1).

To confirm the dissociation constants for Vertex-11e and SCH772984 derived by the kinetic experiments, we used an alternative approach involving a "Morrison-titration" experiment, wherein a fixed concentration of enzyme and substrate are pre-equilibrated with varying concentrations of inhibitors, and the ratio of inhibitor bound to unbound is determined by an enzymatic assay (Figure 4A).[37] The data were fit using eq 3:

$$\frac{v_i}{v_0} = 1 - \frac{[E] + [I] + K_i - \sqrt{([E] + [I] + K_i)^2 - 4[E][I]}}{2[E]}$$

(3)

wherein $[E]$ and $[I]$ are the total concentrations of enzyme and inhibitor, respectively, and $K_i$ is the affinity of the inhibitor for the enzyme. The $K_i$ values from these experiments were 0.34 and 0.12 nM for Vertex-11e and SCH772984, respectively, in good agreement with the $K_d$ values measured independently in the kinetic experiments (Table 1).

We next asked whether the affinities of Vertex-11e or SCH772984 differ between 0P-ERK2 and 2P-ERK2. Such
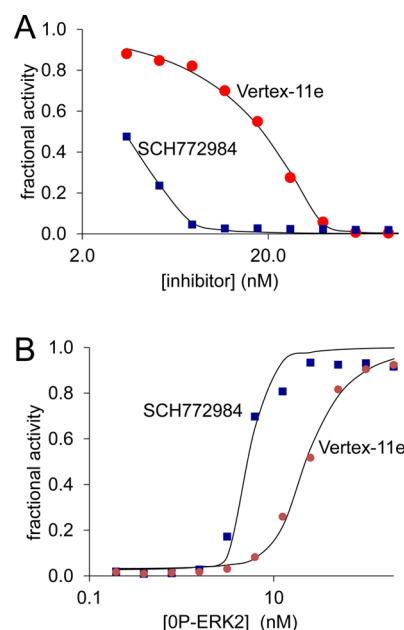
differences might influence the responses of the cell to limiting concentrations of inhibitor, given that the abundance of ERK1/2 in cells is ~1 $\mu$M, and dual phosphorylation in response to cell stimulation rarely reaches 100%. However, it is experimentally challenging to determine affinities for tight-binding compounds from kinetic measurements for enzymes like 0P-ERK2, which have little or no activity. This is true because to measure significant activity, assays must be conducted at high enzyme concentrations, well above the expected binding constant. Therefore, we developed an alternative strategy involving competitive titration, wherein varying concentrations of 0P-ERK2 and fixed concentrations of 2P-ERK2 were mixed and preincubated with nanomolar concentrations of inhibitor, followed by addition of ATP and sub-D to initiate reactions and measurement of phosphoryl transfer by 2P-ERK2. When 0P-ERK2 binds inhibitor, it protects 2P-ERK2 from inhibition without contributing to phosphorylation of substrate; therefore, the initial rate of product formation reflects the relative amount of inhibitor-bound versus free 2P-ERK2. The data can then be fit to two instances of eq 3, the first describing binding of the inhibitor to 0P-ERK2 and the second to 2P-ERK2. The fitting yielded a binding affinity of Vertex-11 for 0P-ERK2 ($K_i = 2.5 \pm 0.5$ nM) that was 1 order of magnitude weaker than that for 2P-ERK2 (0.34 nM) (Figure 4B and Table 1). This suggests that Vertex-11e either adopts distinct modes of binding to 0P-ERK2 versus 2P-ERK2 or binds by conformational selection in which the
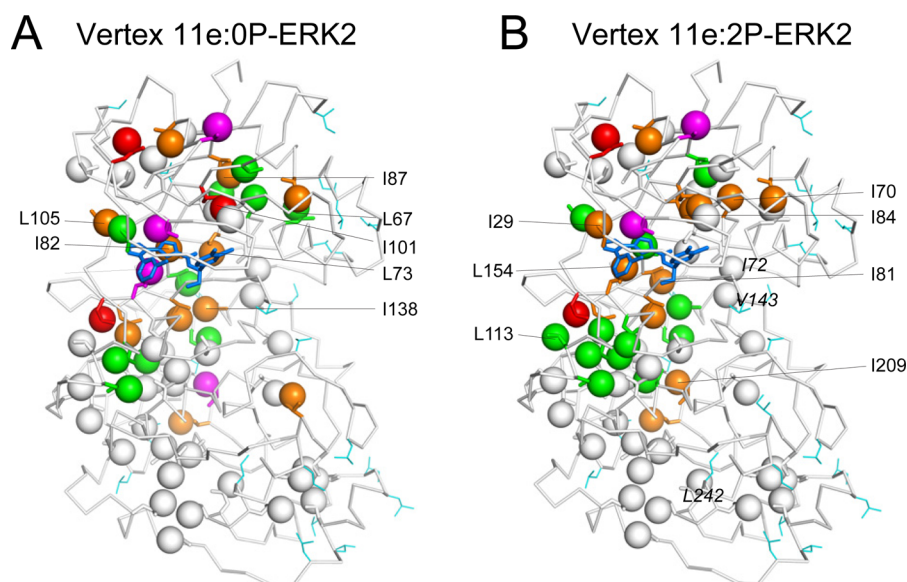
**Figure 5.** Chemical shift perturbations following binding of Vertex-11e to ERK2. (A and B) Ile, Leu, and Val methyls showing $^{13}$C and $^1$H combined chemical shift perturbations induced by binding of Vertex-11e to (A) 0P-ERK2 and (B) 2P-ERK2. The methyls for individual residues were mapped onto a cocrystal structure of 0P-ERK2 and Vertex-9a (blue), an analogue of Vertex-11e (PDB entry 2OJJ[12]). Spheres show Ile, Leu, and Val methyls assigned in the 0P-ERK2 and 2P-ERK2 apoenzymes.[16] Side chains are shown as sticks when the methyl assignment is absent or ambiguous. Colors indicate chemical shift perturbations induced by Vertex-11e binding: <0.05 ppm (white), 0.05−0.1 ppm (green), 0.1−0.2 ppm (orange), and >0.2 ppm (red). Magenta indicates residues with peaks missing in the Vertex-11e−ERK2 complexes, most likely due to changes in methyl dynamics. Labeled residues showed significant differences in chemical shift perturbation upon Vertex-11e binding between ERK2 forms, increasing in 0P-ERK2 (A) or 2P-ERK2 (B) (see Figure S6 of the Supporting Information). In panel B, methyls labeled in italics indicate the positions of I72, V143, and L242, which show no chemical shift perturbation upon binding of Vertex-11e but report the populations of T and R conformers (see Figure 6).
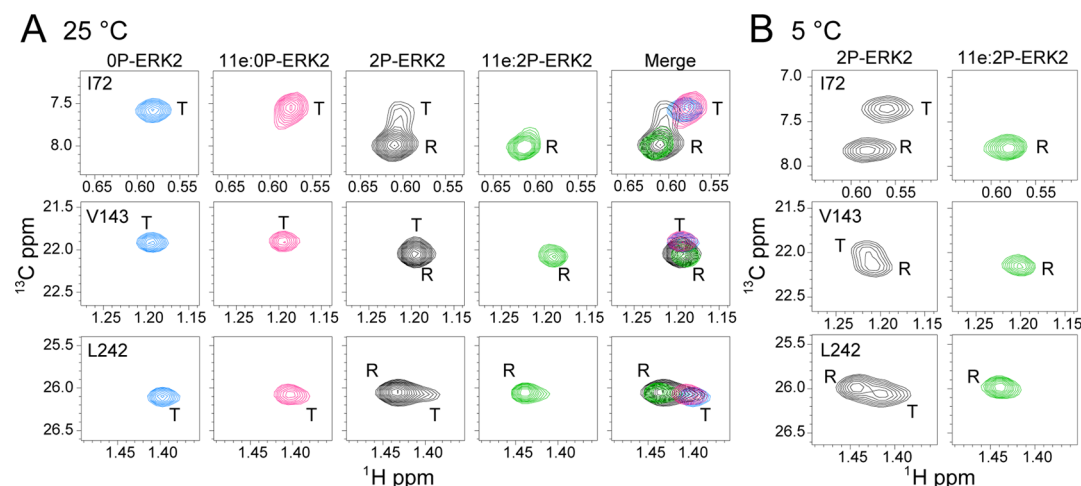


**Figure 6.** Vertex-11e stabilizes the R conformer in 2P-ERK2. (A) 2D $^{13}$C−$^1$H HMQC spectra collected at 25 °C, showing methyl peaks of key residues I72, V143, and L242, which report T and R conformers.[16] Their locations in the structure are shown in Figure 5B. The spectra show that the Vertex-11e−0P-ERK2 complex (pink) adopts the T conformer, observed in the 0P-ERK2 apoenzyme (blue). In contrast, the Vertex-11e−2P-ERK2 complex stabilizes the R conformer (green), shifting the equilibrium between T and R conformers observed in the 2P-ERK2 apoenzyme (black). (B) The same methyl peaks as in panel A, but for spectra collected at 5 °C, showing the more pronounced shift in equilibrium toward the R conformer in the Vertex-11e−2P-ERK2 complex (green), compared to the 2P-ERK2 apoenzyme (black).

binding competent species has very different populations in 0P-ERK2 and 2P-ERK2. In contrast, the binding affinity of SCH772984 for 0P-ERK2 ($K_i$ = 0.12 ± 0.04 nM) equaled that of 2P-ERK2 (0.12 nM). Thus, SCH772984 recognizes each enzyme form with comparable affinity, which validates the structural integrity of 0P-ERK2 in this assay.

To investigate the basis for the differential binding affinities of Vertex-11e for 0P-ERK2 versus 2P-ERK2, we examined responses to Vertex-11e binding by NMR. 2D $^{13}$C−$^1$H HMQC spectra were collected by titrating Vertex-11e into

[methyl-$^1$H,$^{13}$C]Ile-, Leu-, and Val-labeled 0P- and 2P-ERK2 and monitoring the chemical shift changes of 70 labeled residues.[16] The titration ended when peaks reflecting unbound ERK2 were undetectable. The chemical shift perturbations upon binding Vertex-11e occurred at similar residues in 0P-ERK2 and 2P-ERK2 (Figure S6 of the Supporting Information). As summarized in Figure 5, significant chemical shift perturbations were observed throughout the N-terminal lobe as well as the upper C-terminal lobe facing the active site, consistent with Vertex-11e occupancy in the ATP binding

pocket. In detail, however, differences were observable between 0P- and 2P-ERK2 with respect to the magnitude of chemical shift perturbations. The largest differences occurred at residues L67, L73, I82, I87, I101, L105, and I138, which were significantly perturbed in 0P-ERK2 but not 2P-ERK2, and residues I29, I70, I81, I84, L113, L154, and I209, which were significantly perturbed in 2P-ERK2 but not 0P-ERK2 (Figure S6 of the Supporting Information, with residue locations in Figure 5). This reveals different modes of binding of Vertex-11e to the inactive versus active forms of ERK2.

Our previous characterization of ERK2 by *methyl*-($^{13}$C,$^1$H) Carr−Purcell−Meiboom−Gill (CPMG) NMR relaxation dispersion experiments[16] showed that 0P-ERK2 adopts one major conformer (which we will term the "T" conformer, 100%), while 2P-ERK2 undergoes exchange between two different conformers ("T" and "R" conformers, in a 20:80 ratio at 25 °C and a 50:50 ratio at 5 °C). Key residues were found where the chemical shift changes between the two states (in hertz) were larger than the observed chemical exchange rate constant (i.e., $\Delta\omega \gg k_{ex}$), therefore appearing as two peaks in the HMQC spectra of 2P-ERK2. Via comparison of the results of the CPMG to HMQC spectra, the relative intensities for each pair of peaks at these key residues were verified to directly report the relative populations of the T and R conformers.[16]

Examination of these key residues showed that different conformations were formed in the complexes of Vertex-11e with inactive versus active kinase (Figure 6A,B). Whereas binding of Vertex-11e to 0P-ERK2 formed the T conformer seen in the 0P-ERK2 apoenzyme, binding to 2P-ERK2 formed the R conformer. Thus, Vertex-11e favors different conformations in ERK2 depending on the kinase activity state, providing a structural basis for explaining the differential affinities of Vertex-11e for 0P-ERK2 and 2P-ERK2. Importantly, binding of the inhibitor to 2P-ERK2 resulted in a substantial shift in equilibrium between T and R conformers. In its apoenzyme form, 2P-ERK2 interconverts between the T and R conformers, whose equilibrium ratios are 20:80 at 25 °C and 50:50 at 5 °C. Upon ligand binding, the equilibrium shifted completely to the R conformer, at both temperatures. This reveals properties of conformational selection in the active kinase and the capability of inhibitor binding to modulate the thermodynamics of conformational exchange.

## ■ DISCUSSION

Our study reveals two significant insights into the behavior of inhibitors toward ERK2. First, we present a detailed kinetic analysis of inhibition to determine true binding constants as well as association and dissociation rate constants, greatly expanding previous studies that were restricted to measurements of relative potencies ($IC_{50}$) for these inhibitors. From this, we demonstrate that Vertex-11e and SCH772984 display the unexpected properties of slow onset and slow dissociation, distinguishing these two compounds from the other inhibitors. Second, we demonstrate that one of these inhibitors, Vertex-11e, binds with differential affinities to inactive, unphosphorylated (0P) and active, phosphorylated (2P) ERK2. Importantly, the inhibitor forms T-state and R-state conformers with the inactive and active enzyme, respectively. In 2P-ERK2, Vertex-11e binding strongly shifts the equilibrium between T and R conformers to favor the R form. Thus, the allosteric properties of ERK2 endow the active form of the kinase with a novel capability of being inhibited through mechanisms involving conformational selection.

Fast-on and fast-off kinetics were exhibited by four of the molecules examined, including the relatively potent inhibitor FR180204 (Figure 2 and Figures S2−S4 of the Supporting Information). Thus, most inhibitors could be described by classic inhibition kinetics, assessed by the measurement of initial rates. In contrast, both Vertex-11e and SCH772984 displayed hysteresis in the form of time-dependent onset of inhibition and slow dissociation (Figure 3 and Figure S5 of the Supporting Information). The $K_i$ values determined for Vertex-11e and SCH772984 (0.34 and 0.12 nM, respectively) agreed well with $K_d$ values determined previously by temperature-dependent fluorescence and increased thermal stability in the bound form (0.11 and 0.19 nM, respectively),[10] although for unknown reasons they differed significantly from $K_d$ values measured using Bio-Layer Interferometry (85 and 13 nM, respectively).[30] Although the two slow-binding compounds were comparable to each other with respect to their $K_i$ and $K_d$ values, differences were observed in their association and dissociation rate constants, which were 10- and 3-fold slower, respectively, for Vertex-11e than for SCH772984.

These kinetic measurements reveal fundamental differences between ERK inhibitors that are likely to impact cellular function. Characterization of inhibitor molecules during the drug discovery process typically involves $IC_{50}$ determinations, selectivity screening, cell-based assays, and pharmacological absorption, distribution, metabolism, and excretion in animal models. However, a growing body of evidence suggests that residence time, defined as the inverse of $k_{off}$, can also benefit the success of a potential drug, by sustaining pharmacological effects *in vivo*, enhancing on-target occupancy with lower off-target effects, and reducing toxicity from degradation products.[21,22] Our measurements of $k_{off}$ predict long residence times of 4.8 and 0.9 h for Vertex-11e and SCH772984, respectively. As defined by Schramm,[38] an "ultimate physiological inhibitor" would maintain binding until the target is replaced by new protein synthesis. Our key finding that slow kinetics can be achieved for ERK1/2 inhibitors suggests that dissociation rates and residence times would be valuable characteristics to examine in structure−activity studies.

The properties of conformational selection in ERK2 can be linked to the regulation of dynamics induced by dual phosphorylation. Our previous work showed that upon phosphorylation, constraints to dynamics are released in ERK2, to allow equilibrium exchange between T and R conformers. In other words, phosphorylation lowers the thermodynamic barrier for forming the R state, allowing conformational exchange in 2P-ERK2 not seen in 0P-ERK2. Thus, the behavior of Vertex-11e resembles that of type II kinase inhibitors, which work by trapping nonproductive active site conformers. Most type II inhibitors described to date stabilize a kinase inactive conformation, involving a "DFG-out" conformer that disrupts $Mg^{2+}$-ATP binding by distorting the structure of the conserved DFG motif. However, in ERK2, the DFG-out conformation has been achieved only by incorporating multiple mutations, coupled with binding of a type II p38 MAP kinase inhibitor.[39] In its wild-type form, ERK2 shows no indication that the DFG-out conformation is allowed. The crystal structures of 0P-ERK2 bound to Vertex-11e and SCH772984 both clearly show a DFG-in conformation.[30] Thus, it is unlikely that the T and R conformers differ by a DFG flip. Instead, both Vertex-11e and SCH772984 access a novel binding pocket lined by Tyr36 and Tyr54 between helix $\alpha$C and the phosphate binding loop. Mutation of both of these

tyrosines has been shown to increase the rates of dissociation of Vertex-11e and SCH772984 from 0P-ERK2 using Bio-Layer Interferometry.[30] Thus, it appears that Vertex-11e represents a new variant of type II kinase inhibitors, in that it binds tightly but differentially to 0P- and 2P-ERK2, both in the DFG-in conformation. Nevertheless, structural differences between T and R conformers with respect to inhibitor binding mode are clearly indicated by the differences in chemical shift perturbations between Vertex-11e bound to 0P-ERK2 (T) and 2P-ERK2 (R) (Figure 5A,B). Given that all cocrystal structures so far have been determined using 0P-ERK2, future X-ray structures of inhibitors in complex with 2P-ERK2 are needed to determine the structural differences between ligand-bound T and R conformers.

Importantly, Vertex-11e differs from classic type II inhibitors by showing higher selectivity for the R conformer, which is associated with the active state of ERK2. There are two implications of this finding. First, to the extent that the catalytic function of ERK2 involves T ⇌ R interconversion, conformational selection by Vertex-11e would reinforce its ATP competitive effects on kinase inhibition by allowing it to work through a conformational trapping mechanism. Thus, the release of the barrier to dynamics by dual phosphorylation represents a new type of allosteric switch for "type II-like" conformation selective inhibitors to exploit. Second, the behavior of Vertex-11e predicts that it would preferentially bind the active form of ERK2 in cells. This might be advantageous under conditions where tissue levels of inhibitor are limiting, given that the cellular abundance of ERK1/2 typically reaches micromolar concentrations. Preferential binding to the active form of the kinase would minimize competition for inhibitor by the larger pool of inactive ERK. We propose that the T ⇌ R conformational equilibrium in ERK2 provides a new property to exploit in structure–activity studies, which can impact inhibitor mechanism and cellular potency.

Finally, we asked about the degree to which T ⇌ R conformational exchange accounts for the property of slow dissociation in Vertex-11e. Conformational selection has been associated with long residence times and inhibitor potency. For example, slow off rates have been reported for p38, MET, IGF1R, and VEGFR inhibitors and ascribed to their selective binding to the DFG-out conformation.[40−44] Slow dissociation and a higher rate of cell retention of ponatinib have also been used to explain its higher potency toward BCR-ABL in primary acute myeloid leukemia cells.[18] Thus, conformational selection in kinase inhibitors may prove to be a valuable means of conferring slow tight binding, leading to higher potency and cellular efficacy.[45] Initially, we suspected that the slow association or dissociation of Vertex-11e and SCH772984 might be explained by the interconversion between T and R conformers. The most commonly observed mechanism for slow tight binding is a two-step model in which enzyme and inhibitor associate rapidly followed by a slow conformational change to a tight-binding complex (E + I ⇌ EI ⇌ EI*).[46,47] However, two observations argue against this model here. First, the kinetics of both Vertex-11e and SCH772984 are most consistent with a one-step mechanism to form a tight-binding complex (E + I ⇌ EI*). Although less common than the two-step model, the one-step model has been observed for other tight-binding protein kinase inhibitors.[48,49] Second, previous NMR CPMG studies of the 2P-ERK2 apoenzyme measured rate constants for T ⇌ R exchange of 240 and 60 s$^{-1}$ in the

forward and reverse directions, respectively. Therefore, it is unlikely that the slow association or dissociation of Vertex-11e is rate-limited by T ⇌ R interconversion. Instead, T and R interconvert rapidly in 2P-ERK2 prior to inhibitor binding, and the slow kinetics of binding and dissociation are most likely attributed to structural features in the R conformer, which remain to be determined. Further studies are needed to understand the structural basis of slow inhibition and examine the linkage between allostery and kinetics in ERK2.

## ■ ASSOCIATED CONTENT

### ⑤ Supporting Information

Determinations of $K_m$ values for ATP and peptide substrate (Figure S1), representative data for time-dependent assays of a rapid on/off inhibitor of ERK2, olomoucin (Figure S2), representative data for time-dependent assays of a rapid on/off inhibitor of ERK2, SB220025 (Figure S3), representative data for time-dependent assays of a rapid on/off inhibitor of ERK2, Vertex-1 (Figure S4), representative data for a time-dependent inhibitor of ERK2, SCH772984 (Figure S5), and chemical shift perturbations upon binding of Vertex-11e to ERK2 (Figure S6). This material is available free of charge via the Internet at http://pubs.acs.org.

## ■ AUTHOR INFORMATION

### Corresponding Author

*Department of Chemistry and Biochemistry, University of Colorado, Boulder, CO 80309. E-mail: natalie.ahn@colorado.edu. Phone: (303) 492-4799.

### Notes

The authors declare no competing financial interest.

## ■ ABBREVIATIONS

ERK, extracellular signal-regulated kinase; MAP, mitogen-activated protein; 0P-ERK2, unphosphorylated ERK2; 2P-ERK2, dually phosphorylated ERK2; MKK, MAP kinase kinase; PDB, Protein Data Bank.

## ■ REFERENCES

(1) Roberts, P. J., and Der, C. J. (2007) Targeting the Raf-MEK-ERK mitogen-activated protein kinase cascade for the treatment of cancer. *Oncogene 26*, 3291−3310.

(2) Flaherty, K. T., Hodi, F. S., and Bastian, B. C. (2010) Mutation-driven drug development in melanoma. *Curr. Opin. Oncol. 22*, 178−183.

(3) Solit, D. B., and Rosen, N. (2011) Resistance to BRAF inhibition in melanomas. *N. Engl. J. Med. 364*, 772−774.

(4) Flaherty, K. T., Infante, J. R., Daud, A., Gonzalez, R., Kefford, R. F., Sosman, J., Hamid, O., Schuchter, L., Cebon, J., Ibrahim, N., Kudchadkar, R., Burris, H. A., III, Falchook, G., Algazi, A., Lewis, K., Long, G. V., Puzanov, I., Lebowitz, P., Singh, A., Little, S., Sun, P., Allred, A., Ouellet, D., Kim, K. B., Patel, K., and Weber, J. (2012) Combined BRAF and MEK inhibition in melanoma with BRAF V600 mutations. *N. Engl. J. Med. 367*, 1694−1703.

(5) Ribas, A., Gonzalez, R., Pavlick, A., Hamid, O., Gajewski, T. F., Daud, A., Flaherty, L., Logan, T., Chmielowski, B., Lewis, K., Kee, D., Boasberg, P., Yin, M., Chan, I., Musib, L., Choong, N., Puzanov, I., and McArthur, G. A. (2014) Combination of vemurafenib and cobimetinib

in patients with advanced BRAF(V600)-mutated melanoma: A phase 1b study. *Lancet Oncol. 15*, 954−965.

(6) Nazarian, R., Shi, H., Wang, Q., Kong, X., Koya, R. C., Lee, H., Chen, Z., Lee, M. K., Attar, N., Sazegar, H., Chodon, T., Nelson, S. F., McArthur, G., Sosman, J. A., Ribas, A., and Lo, R. S. (2010) Melanomas acquire resistance to B-RAF(V600E) inhibition by RTK or N-RAS upregulation. *Nature 468*, 973−977.

(7) Little, A. S., Balmanno, K., Sale, M. J., Newman, S., Dry, J. R., Hampson, M., Edwards, P. A. W., Smith, P. D., and Cook, S. J. (2011) Amplification of the driving oncogene, KRAS or BRAF, underpins acquired resistance to MEK1/2 inhibitors in colorectal cancer cells. *Sci. Signaling 4*, ra17.

(8) Greger, J. G., Eastman, S. D., Zhang, V., Bleam, M. R., Hughes, A. M., Smitheman, K. N., Dickerson, S. H., Laquerre, S. G., Liu, L., and Gilmer, T. M. (2012) Combinations of BRAF, MEK, and PI3K/mTOR inhibitors overcome acquired resistance to the BRAF inhibitor GSK2118436 dabrafenib, mediated by NRAS or MEK mutations. *Mol. Cancer Ther. 11*, 909−920.

(9) Shi, H., Moriceau, G., Kong, X., Lee, M. K., Lee, H., Koya, R. C., Ng, C., Chodon, T., Scolyer, R. A., Dahlman, K. B., Sosman, J. A., Kefford, R. F., Long, G. V., Nelson, S. F., Ribas, A., and Lo, R. S. (2012) Melanoma whole-exome sequencing identifies (V600E)B-RAF amplification-mediated acquired B-RAF inhibitor resistance. *Nat. Commun. 3*, 724.

(10) Morris, E. J., Jha, S., Restaino, C. R., Dayananth, P., Zhu, H., Cooper, A., Carr, D., Deng, Y., Jin, W., Black, S., Long, B., Liu, J., Dinunzio, E., Windsor, W., Zhang, R., Zhao, S., Angagaw, M. H., Pinheiro, E. M., Desai, J., Xiao, L., Shipps, G., Hruza, A., Wang, J., Kelly, J., Paliwal, S., Gao, X., Babu, B. S., Zhu, L., Daublain, P., Zhang, L., Lutterbach, B. A., Pelletier, M. R., Philippar, U., Siliphaivanh, P., Witter, D., Kirschmeier, P., Bishop, W. R., Hicklin, D., Gilliland, D. G., Jayaraman, L., Zawel, L., Fawell, S., and Samatar, A. A. (2013) Discovery of a novel ERK inhibitor with activity in models of acquired resistance to BRAF and MEK inhibitors. *Cancer Discovery 3*, 742−750.

(11) Hatzivassiliou, G., Liu, B., O'Brien, C., Spoerke, J. M., Hoeflich, K. P., Haverty, P. M., Soriano, R., Forrest, W. F., Heldens, S., Chen, H., Toy, K., Ha, C., Zhou, W., Song, K., Friedman, L. S., Amler, L. C., Hampton, G. M., Moffat, J., Belvin, M., and Lackner, M. R. (2012) ERK inhibition overcomes acquired resistance to MEK inhibitors. *Mol. Cancer Ther. 11*, 1143−1153.

(12) Aronov, A. M., Tang, Q., Martinez-Botella, G., Bemis, G. W., Cao, J., Chen, G., Ewing, N. P., Ford, P. J., Germann, U. A., Green, J., Hale, M. R., Jacobs, M., Janetka, J. W., Maltais, F., Markland, W., Namchuk, M. N., Nanthakumar, S., Poondru, S., Straub, J., ter Haar, E., and Xie, X. (2009) Structure-guided design of potent and selective pyrimidylpyrrole inhibitors of extracellular signal-regulated kinase (ERK) using conformational control. *J. Med. Chem. 52*, 6362−6368.

(13) Zhang, F., Strand, A., Robbins, D., Cobb, M. H., and Goldsmith, E. J. (1994) Atomic structure of the MAP kinase ERK2 at 2.3 Å resolution. *Nature 367*, 704−711.

(14) Canagarajah, B. J., Khokhlatchev, A., Cobb, M. H., and Goldsmith, E. J. (1997) Activation mechanism of the MAP kinase ERK2 by dual phosphorylation. *Cell 90*, 859−869.

(15) Prowse, C. N., and Lew, J. (2001) Mechanism of Activation of ERK2 by Dual Phosphorylation. *J. Biol. Chem. 276*, 99−103.

(16) Xiao, Y., Lee, T., Latham, M. P., Warner, L. R., Tanimoto, A., Pardi, A., and Ahn, N. G. (2014) Phosphorylation releases constraints to domain motion in ERK2. *Proc. Natl. Acad. Sci. U.S.A. 111*, 2506−2511.

(17) Zhao, Z., Wu, H., Wang, L., Liu, Y., Knapp, S., Liu, Q., and Gray, N. S. (2014) Exploration of Type II Binding Mode: A Privileged Approach for Kinase Inhibitor Focused Drug Discovery? *ACS Chem. Biol. 9*, 1230−1241.

(18) Lovering, F., McDonald, J., Whitlock, G. A., Glossop, P. A., Phillips, C., Bent, A., Sabnis, Y., Ryan, M., Fitz, L., Lee, J., Chang, J. S., Han, S., Kurumbail, R., and Thorarensen, A. (2012) Identification of type-II inhibitors using kinase structures. *Chem. Biol. Drug Des. 80*, 657−664.

(19) Wood, E. R., Truesdale, A. T., McDonald, O. B., Yuan, D., Hassell, A., Dickerson, S. H., Ellis, B., Pennisi, C., Horne, E., Lackey, K., Alligood, K. J., Rusnak, D. W., Gilmer, T. M., and Shewchuk, L. (2004) A unique structure for epidermal growth factor receptor bound to GW572016 (Lapatinib): Relationships among protein conformation, inhibitor off-rate, and receptor activity in tumor cells. *Cancer Res. 64*, 6652−6659.

(20) Palmieri, L., and Rastelli, G. (2013) αC helix displacement as a general approach for allosteric modulation of protein kinases. *Drug Discovery Today 18*, 407−414.

(21) Copeland, R. A., Pompliano, D. L., and Meek, T. D. (2006) Drug-target residence time and its implications for lead optimization. *Nat. Rev. Drug Discovery 5*, 730−739.

(22) Copeland, R. A. (2011) Conformational adaptation in drug−target interactions and residence time. *Future Med. Chem. 3*, 1491−1501.

(23) Francis, D. M., et al. (2011) Resting and active states of the ERK2:HePTP complex. *J. Am. Chem. Soc. 133*, 17138−17141.

(24) Shapiro, P. S., et al. (1998) Activation of the MKK/ERK pathway during somatic cell mitosis: Direct interactions of active ERK with kinetochores and regulation of the mitotic 3F3/2 phosphoantigen. *J. Cell Biol. 142*, 1533−1545.

(25) Delaglio, F., Grzesiek, S., Vuister, G. W., Zhu, G., Pfeifer, J., and Bax, A. (1995) NMRPipe: A multidimensional spectral processing system based on UNIX pipes. *J. Biomol. NMR 6*, 277−293.

(26) Vranken, W. F., Boucher, W., Stevens, T. J., Fogh, R. H., Pajon, A., Llinas, M., Ulrich, E. L., Markley, J. L., Ionides, J., and Laue, E. D. (2005) The CCPN data model for NMR spectroscopy: Development of a software pipeline. *Proteins 59*, 687−696.

(27) Wang, Z., Canagarajah, B. J., Boehm, J. C., Kassisá, S., Cobb, M. H., Young, P. R., Abdel-Meguid, S., Adams, J. L., and Goldsmith, E. J. (1998) Structural basis of inhibitor selectivity in MAP kinases. *Structure 6*, 1117−1128.

(28) Ohori, M., Kinoshita, T., Okubo, M., Sato, K., Yamazaki, A., Arakawa, H., Nishimura, S., Inamura, N., Nakajima, H., Neya, M., Miyake, H., and Fujii, T. (2005) Identification of a selective ERK inhibitor and structural determination of the inhibitor−ERK2 complex. *Biochem. Biophys. Res. Commun. 336*, 357−363.

(29) Aronov, A. M., Baker, C., Bemis, G. W., Cao, J., Chen, G., Ford, P. J., Germann, U. A., Green, J., Hale, M. R., Jacobs, M., Janetka, J. W., Maltais, F., Martinez-Botella, G., Namchuk, M. N., Straub, J., Tang, Q., and Xie, X. (2007) Flipped Out: Structure-Guided Design of Selective Pyrazolylpyrrole ERK Inhibitors. *J. Med. Chem. 50*, 1280−1287.

(30) Chaikuad, A., Tacconi, E. M. C., Zimmer, J., Liang, Y., Gray, N. S., Tarsounas, M., and Knapp, S. (2014) A unique inhibitor binding site in ERK1/2 is associated with slow binding kinetics. *Nat. Chem. Biol. 10*, 853−860.

(31) Humphrey, W., Dalke, A., and Schulten, K. (1996) VMD: Visual Molecular Dynamics. *J. Mol. Graphics 14*, 33−38.

(32) Fernandes, N., Bailey, D. E., VanVranken, D. L., and Allbritton, N. L. (2007) Use of docking peptides to design modular substrates with high efficiency for mitogen-activated protein kinase extracellular signal-regulated kinase. *ACS Chem. Biol. 2*, 665−673.

(33) Lee, S., Warthaka, M., Yan, C., Kaoud, T., Ren, P., and Dalby, K. N. (2011) Examining docking interactions on Erk2 with modular peptide substrates. *Biochemistry 50*, 9500−9510.

(34) Morrison, J. F., and Walsh, C. T. (1988) The behavior and significance of slow-binding enzyme inhibitors. *Adv. Enzymol. 61*, 201−301.

(35) Cha, S. (1975) Tight-binding inhibitors I: Kinetic behavior. *Biochem. Pharmacol. 24*, 2177−2185.

(36) Copeland, R. A. (2013) *Evaluation of enzyme inhibitors in drug discovery*, John Wiley & Sons, Hoboken, NJ.

(37) Morrison, J. F. (1969) Kinetics of the reversible inhibition of enzyme-catalyzed reactions by tight-binding inhibitors. *Biochim. Biophys. Acta 185*, 269−286.

(38) Lewandowicz, A., Tyler, P. C., Evans, G. B., Furneaux, R. H., and Schramm, V. L. (2003) Achieving the ultimate physiological goal in

transition state analogue inhibitors for purine nucleoside phosphorylase. *J. Biol. Chem. 278*, 31465−31468.

(39) Hari, S. B., Merritt, E. A., and Maly, D. J. (2013) Sequence determinants of a specific inactive protein kinase conformation. *Chem. Biol. 20*, 806−815.

(40) Millan, D. S., Bunnage, M. E., Burrows, J. L., Butcher, K. J., Dodd, P. G., Evans, T. J., Fairman, D. A., Hughes, S. J., Kilty, I. C., Lemaitre, A., Lewthwaite, R. A., Mahnke, A., Mathias, J. P., Philip, J., Smith, R. T., Stefaniak, M. H., Yeadon, M., and Phillips, C. (2011) Design and synthesis of inhaled p38 inhibitors for the treatment of chronic obstructive pulmonary disease. *J. Med. Chem. 54*, 7797−7814.

(41) Yan, S. B., Peek, V. L., Ajamie, R., Buchanan, S. G., Graff, J. R., Heidler, S. A., Hui, Y. H., Huss, K. L., Konicek, B. W., Manro, J. R., Shih, C., Stewart, J. A., Stewart, T. R., Stout, S. L., Uhlik, M. T., Um, S. L., Wang, Y., Wu, W., Yan, L., Yang, W. J., Zhong, B., and Walgren, R. A. (2013) LY2801653 is an orally bioavailable multi-kinase inhibitor with potent activity against MET, MST1R, and other oncoproteins, and displays anti-tumor activities in mouse xenograft models. *Invest. New Drugs 31*, 833−844.

(42) Lesuisse, D., Mauger, J., Nemecek, C., Maignan, S., Boiziau, J., Harlow, G., Hittinger, A., Ruf, S., Strobel, H., Nair, A., Ritter, K., Malleron, J. L., Dagallier, A., El-Ahmad, Y., Guilloteau, J. P., Guizani, H., Bouchard, H., and Venot, C. (2011) Discovery of the first non-ATP competitive IGF-1R kinase inhibitors: Advantages in comparison with competitive inhibitors. *Bioorg. Med. Chem. Lett. 21*, 2224−2228.

(43) Iwata, H., Imamura, S., Hori, A., Hixon, M. S., Kimura, H., and Miki, H. (2011) Biochemical characterization of a novel type-II VEGFR2 kinase inhibitor: Comparison of binding to non-phosphorylated and phosphorylated VEGFR2. *Bioorg. Med. Chem. 19*, 5342−5351.

(44) Iwata, H., Imamura, S., Hori, A., Hixon, M. S., Kimura, H., and Miki, H. (2011) Biochemical characterization of TAK-593, a novel VEGFR/PDGFR inhibitor with a two-step slow binding mechanism. *Biochemistry 50*, 738−751.

(45) Hu, Y., Furmann, N., and Bajorath, J. (2014) Current compound coverage of the kinome. *J. Med. Chem.*, DOI: 10.1021/jm5008159.

(46) Schloss, J. V. (1988) Significance of slow-binding enzyme inhibition and its relationship to reaction-intermediate analogues. *Acc. Chem. Res. 21*, 348−353.

(47) Baici, A. (2012) Slow-onset Enzyme Inhibition and Inactivation. In *Proceedings of the 5th Beilstein ESCEC Symposium*, Beilstein Institute: Rüdesheim/Rhein, Germany, pp 55−73.

(48) Mason, J. L., Spais, C., Husten, J., Prouty, E., Albom, M. S., Meyer, S. L., Ator, M. A., and Angeles, T. S. (2012) Comparison of LanthaScreen Eu Kinase Binding Assay and Surface Plasmon Resonance Method in Elucidating the Binding Kinetics of Focal Adhesion Kinase Inhibitors. *Assay Drug Dev. Technol. 10*, 468−475.

(49) Millan, D. S., Bunnage, M. E., Burrows, J. L., Butcher, K. J., Dodd, P. G., Evans, T. J., Fairman, D. A., Hughes, S. J., Kilty, I. C., Lemaitre, A., Lewthwaite, R. A., Mahnke, A., Mathias, J. P., Philip, J., Smith, R. T., Stefaniak, M. H., Yeadon, M., and Phillips, C. (2011) Design and Synthesis of Inhaled p38 Inhibitors for the Treatment of Chronic Obstructive Pulmonary Disease. *J. Med. Chem. 54*, 7797−7814.